

# Temperature dependence of conductance fluctuations in quantum Hall multilayers

H. A. Walling,<sup>1</sup> E. G. Gwinn,<sup>1</sup> J. Xu,<sup>1</sup> K. D. Maranowski,<sup>2</sup> and A. C. Gossard<sup>2</sup>

<sup>1</sup>Physics Department, UCSB, Santa Barbara, California 93106, USA

<sup>2</sup>Materials and ECE Departments, UCSB, Santa Barbara, California 93106, USA

(Received 15 December 2003; revised manuscript received 14 July 2004; published 30 December 2004)

We study conductance fluctuations in low-temperature, vertical transport through quantum Hall multilayers. The mesas studied are fabricated from a 50-period multilayer in which 150 Å GaAs wells alternate with 150 Å AlGaAs barriers that are delta-doped at their centers. We find qualitatively different temperature dependences of the variance,  $\delta G^2$ , measured near the centers of the  $\nu=2$  and  $\nu=1$  quantum Hall states, with non-monotonic variation in  $\delta G^2(T)$  at  $\nu=1$ . The observed temperature dependence of the correlation field is also surprising in light of theoretical predictions for fluctuations of the edge state sheath. Including the temperature dependence of the mean conductance and the effects of flux cancellation improves agreement between observed and predicted temperature dependences.

DOI: 10.1103/PhysRevB.70.235343

PACS number(s): 73.43.-f

The phenomenon of “universal” conductance fluctuations<sup>1</sup> is a well-known tool for studying electron-dephasing processes in metallic systems. These reproducible fluctuations arise in disordered systems, where electrons can take multiple paths through scattering sites, resulting in quantum interference. Varying an applied magnetic field changes the flux linked through the interfering paths. The result of this change in their phase differences is a reproducible pattern of conductance fluctuations unique to the disorder potential in the sample. The designation “universal” refers to the zero-temperature variance,  $\delta G^2$ , of the fluctuations, which is on the order of  $(e^2/h)^2$  in metals. At finite temperature ( $T$ ), phase coherence lengths shorten and quantum interference effects are muted as electrons dephase through inelastic phonon and electron-electron scattering. As a result,  $\delta G^2$  in metallic systems decrease as  $T$  increases. Characterizing the behavior of  $\delta G^2$  as a function of temperature, then, provides information on electron dephasing.

Here we study the temperature dependence of reproducible conductance fluctuations in quantum Hall multilayers. The vertical transport mesas we study are bounded by an unusual 2D system, a chiral sheath of coupled edge states [Fig. 1(a)]. This surface phase dominates vertical transport at low temperatures that freeze out parallel bulk transport.<sup>2,3</sup>

While other groups<sup>4–9</sup> studied conductance fluctuations in in-plane transport in single-layer quantum Hall (QH) samples, these earlier experiments generally focused on transition regions between QH states. In contrast, our vertical transport samples allow us to study conductance fluctuations within QH states. We study smaller samples than reported on previously<sup>10</sup> to amplify the fluctuations relative to the mean and to move closer to the coherent limit at low  $T$ . We find a striking difference in behavior between the  $\nu=1$  and  $\nu=2$  QH states and from the behavior of conventional metallic systems.

We use 5  $\mu\text{m}$ , 10  $\mu\text{m}$ , 150  $\mu\text{m}$ , and 1 mm-per-side square mesas to study conductance fluctuations in the vertical conductance,  $G_{zz}$ , at the centers of the  $\nu=1$  and  $\nu=2$  quantum Hall states. Here,  $\nu=1$  refers to the QH state for which the Fermi energy lies between the spin-split extended

states of the lowest Landau band of the multilayer, as identified by the value of the in-plane Hall resistance of a companion in-plane transport sample.<sup>2</sup> The MBE-grown multilayer has  $N_{\text{layer}}=50$  layers of 150 Å GaAs quantum wells alternating with 150 Å Al<sub>0.10</sub>Ga<sub>0.90</sub>As barriers. The multilayer period,  $a$ , is 300 Å and the total multilayer height,  $H$ , is 1.5  $\mu\text{m}$ . The barriers are delta-doped with Si to give the wells a carrier concentration of  $2.5 \times 10^{11}/\text{cm}^2$ . Layers of degenerately doped  $n+$  GaAs sandwich the multilayer. We used electron-beam lithography to define the smaller mesas. The top Ni/Au/Ge Ohmic contact metallization served as an etch mask for a SiCl<sub>4</sub> dry etch that stopped within the bottom  $n+$  contact layer. After depositing Ni/Au/Ge bottom contacts, we alloyed the samples at 430 °C for one minute in a rapid thermal annealer.

In this study, the applied field,  $B$ , is perpendicular to the planes of the multilayer. We measure  $G_{zz}$  at dilution refrigerator temperatures by voltage biasing the sample and using

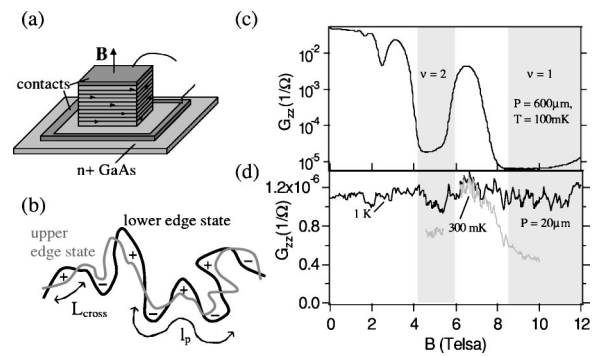


FIG. 1. (a) Schematic of a multilayer mesa. (b) Schematic of the projection of the paths of two adjacent edge states onto the plane.  $L_{\text{cross}}$  is the average distance between projected crossings and  $l_p$  is the phase coherence length along the edge. Successive area elements between the edge states link flux increments with alternating sign on each crossing. (c)  $G_{zz}$  as a function of magnetic field for a large mesa with nominal perimeter  $P_0=600 \mu\text{m}$  at 100 mK. Conductance fluctuations are hardly noticeable. (d)  $G_{zz}$  as a function of magnetic field for a small mesa with nominal perimeter  $P_0=20 \mu\text{m}$  at 1 K (black) and 300 mK (grey).

lock-in techniques at 5 Hz to measure the current as we slowly sweep the perpendicular magnetic field,  $B$ . We avoid electron heating by using small excitation voltages ( $8.9 \mu\text{V}$ , or  $\sim 6 \times 10^{-17} \text{ W}$  at 70 mK) and low sweep rates (0.1 Tesla/minute), and collect each data point after leaving the field static for a time following the sweep from  $B$  to  $B + \delta B$ . In the  $\nu=2$  (1) quantum Hall state, we use a field spacing,  $\delta B$ , of 0.002 (0.0033) T. We sweep  $B$  across the central region of these quantum Hall states, for  $\nu=2$ , from 4.6 to 5.4 T, and for  $\nu=1$ , from 9.0 to 10.0 T.

Figure 1(c) shows  $G_{zz}$  measured at 100 mK on a square mesa with nominal perimeter  $P_0=600 \mu\text{m}$ . This large sample has indistinguishably small conductance fluctuations on the scale of the plot. The deep minima in  $G_{zz}$  are the QH states. At low fields and at the peaks in  $G_{zz}$  between QH states,  $G_{zz}$  is weakly  $T$ -dependent and scales with mesa area,  $A$ , as expected for charge flow throughout the bulk of the mesa for fields corresponding to nearly metallic behavior. In high fields,  $G_{zz}=G_{\text{bulk}}+G_{\text{sheath}}$  has a contribution  $G_{\text{bulk}}$  from the bulk and  $G_{\text{sheath}}$  from the edge state sheath. Within QH states,  $G_{\text{bulk}}$  freezes out at low  $T$  and  $G_{zz} \cong G_{\text{sheath}}$  approaches a constant value that scales with the mesa perimeter.

Figure 1(d) plots  $G_{zz}$  measured at 1 K, using a coarse field resolution, in a small square mesa with nominal perimeter  $P_0=20 \mu\text{m}$ . The  $G_{zz}$  axis is linear rather than logarithmic, as in Fig. 1(c). By size scaling we expect  $G_{\text{bulk}}$  reduced by a factor of 900 and  $G_{\text{sheath}}$  reduced by a factor of 30 relative to the  $150\text{-}\mu\text{m} \times 150\text{-}\mu\text{m}$  mesa of Fig. 1(c), at the same temperature. In the weakly  $T$ -dependent regions between QH states, the observed reduction in  $G_{zz}$  between the smaller and larger samples is roughly as expected for bulk-dominated transport. The average  $G_{zz}$  in the  $\nu=2$  QH state in the small mesa displays roughly the expected<sup>2,11</sup> drop in  $G_{zz}$ , assuming sheath-dominated conductance in both samples. As shown in Fig. 1(d),  $G_{zz}$  in the small mesa fluctuates strongly across the entire field range. In the following discussion, we concentrate on fluctuations within the QH states.

If adjacent edge states perfectly overlaid, a perpendicular applied  $B$  would not link flux through the surface sheath. However, due to surface roughness and disorder, the lateral boundaries of the electron gases in different layers will not perfectly overlaid [Fig. 1(b)]. Such relative displacement of edge states in adjacent layers links flux from a vertical field, producing phase shifts that result in fluctuations in  $G_{\text{sheath}}$ . Previous tilted-field experiments<sup>12</sup> confirmed that a magnetic field perpendicular to the layers does cause  $G_{zz}$  to fluctuate.

Figures 2(a) and 2(b) show  $G_{zz}$  as a function of  $B$  between  $T=70 \text{ mK}$  and 1 K in the  $\nu=1$  and  $\nu=2$  QH states, respectively. We note the presence of fine and coarse field-scale features in both states. We also observe that in the  $\nu=1$  state, the fluctuations at high  $T$  have noticeably larger amplitudes than those at low  $T$ , in contrast to what we expect from conductance fluctuations due to quantum interference in conventional metallic systems.

To quantify the temperature dependence of conductance fluctuations, we use the correlation function  $F(B, \delta B) = \langle [G_{zz}(B) - \langle G_{zz}(B) \rangle][G_{zz}(B + \delta B) - \langle G_{zz}(B + \delta B) \rangle] \rangle$ , where  $G_{zz}$  is the measured vertical conductance and  $\langle G_{zz}(B) \rangle$  is the field-dependent mean.  $F(B, \delta B)$  yields the variance,  $\delta G^2$ , and

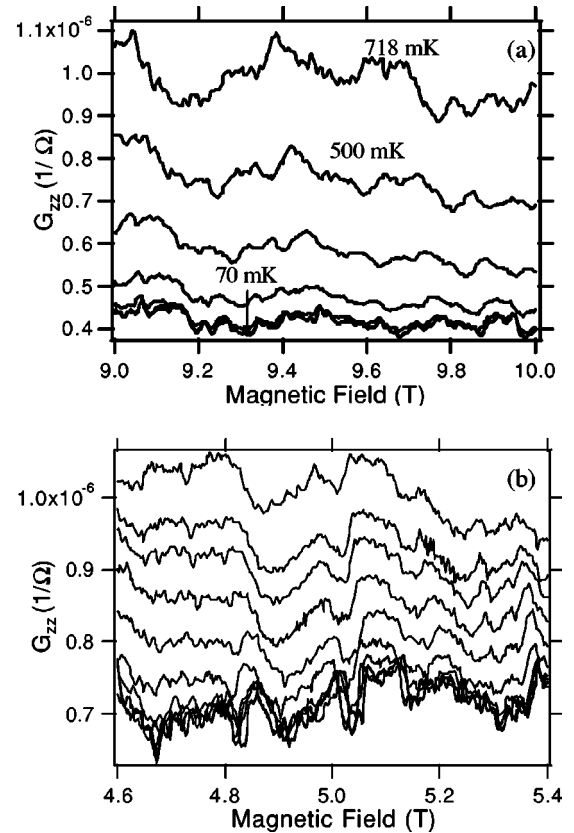


FIG. 2. Conductance fluctuations as a function of temperature for (a)  $\nu=1$  and (b)  $\nu=2$ . The curves correspond, from top to bottom for  $\nu=1$ , to  $T=718, 500, 400, 300, 200, 100,$  and  $70 \text{ mK}$ . For  $\nu=2$ , from top to bottom,  $T=1 \text{ K}, 800, 700, 600, 500, 400, 300, 200, 140, 100,$  and  $70 \text{ mK}$ .

the correlation field,  $B_c$ , of the fluctuations in  $G_{zz}$ . The calculation of  $F$  in the QH states is complicated by factors that do not arise in studies of metal films. The range of fields available for calculating  $F$  is limited by the width of the QH state, which in turn limits the accuracy of  $F$ . Calculation of  $F$  is also complicated by the non-negligible field and  $T$  dependences of the mean conductance,  $\langle G_{zz} \rangle$ .

The first step we take to calculate  $F(B, \delta B)$  from the data is to remove  $\langle G_{zz}(B) \rangle$  from the total conductance,  $G_{zz}(B)$ . If the estimated  $\langle G_{zz}(B) \rangle$  follows  $G_{zz}$  too closely, we remove some fluctuations in addition to the mean. On the other hand, an estimated  $\langle G_{zz}(B) \rangle$  that varies more slowly with field than the true  $\langle G_{zz}(B) \rangle$  will overestimate the fluctuations. We have examined the effects of several different ways of estimating  $\langle G_{zz}(B) \rangle$ , and find that our results for the variance and correlation fields that we extract from  $F$  as described below are similar across all techniques that we studied,<sup>13</sup> as shown in Fig. 4.

Figure 3 shows conductance data for  $\nu=2$  at 200 mK (black curve) with two different estimates of  $\langle G_{zz}(B) \rangle$  (gray curves). The “loose” fit for  $\langle G_{zz} \rangle$  uses a running average over a field range of 0.10 T in  $\nu=2$  and 0.17 T in  $\nu=1$  (light gray); “tight” refers to the running average over a shorter field range, 0.04 T in  $\nu=2$  and 0.067 T in  $\nu=1$  (dark gray).

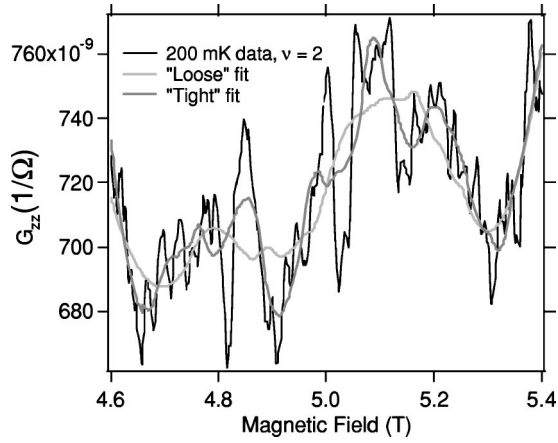


FIG. 3. Conductance fluctuations for  $\nu=2$  at 200 mK (black) with “loose” (light gray) and “tight” (dark gray) estimates of  $\langle G_{zz}(B) \rangle$ . The corresponding correlation functions are shown in Fig. 4 (top).

The results in Fig. 4 show that the parameters extracted from the correlation function,  $F$ , are not very sensitive to the method used to estimate  $\langle G_{zz} \rangle$ . Both the “loose” and “tight” estimates of  $\langle G_{zz} \rangle$  yield similar variance and correlation field,  $B_c$ , as do estimating  $\langle G_{zz} \rangle$  as the best-fit straight line across the field range of the calculation (“line” in Fig. 4) and estimating  $\langle G_{zz} \rangle$  as the best-fit tenth-order polynomial (“poly10” in Fig. 4).

With  $\langle G_{zz}(B) \rangle$  removed, we calculate  $F(\delta B)$ , which we fit to a Lorentzian form,  $F(\delta B) = C + \langle \delta G^2 \rangle / [1 + (\delta B / B_c)^2]$ , where  $\langle \delta G^2 \rangle$  is the fitted variance and  $B_c$  is the fitted correlation field. The constant  $C$  largely absorbs the effects of systematic errors in the estimate of the mean: different techniques for estimating  $\langle G_{zz}(B) \rangle$  give different  $C$  but similar  $\langle \delta G^2 \rangle$  and  $B_c$ . We find an excellent fit to this offset Lorentzian form, as illustrated in Figs. 4(a) ( $\nu=1$ ) and 4(b) ( $\nu=2$ ), which show the results of calculating  $F$  for the two different mean estimates in Fig. 3. The shapes of the  $F(\delta B)$  curves are nearly identical, as shown in Fig. 4, and yield similar  $\langle \delta G^2 \rangle$  and  $B_c$ .

To estimate the uncertainty in the fitted values of  $\langle \delta G^2 \rangle$  and  $B_c$ , we form simulated data sets and analyze them exactly as we do the experimental data. We generate Lorentzian-correlated simulated data by convolving a Lorentzian window with a sequence of random numbers drawn from a Gaussian distribution. The width of the window and the number of points in the simulated data are chosen to correspond to the ratio of the field range of the experimental data to the fitted  $B_c$ . To simulate the effects of our mean removal process, we add a fourth-order polynomial, similar in shape to the overall trend in  $G_{zz}(B)$ , to the simulated fluctuations. Finally, we use each mean removal algorithm to remove the corresponding estimate of the mean from the fluctuations, and calculate the correlation function. We repeat this process for 100 simulated data sets, and average the resulting variances and correlation fields. We use the standard deviations of these averages as the error bars in Fig. 4.

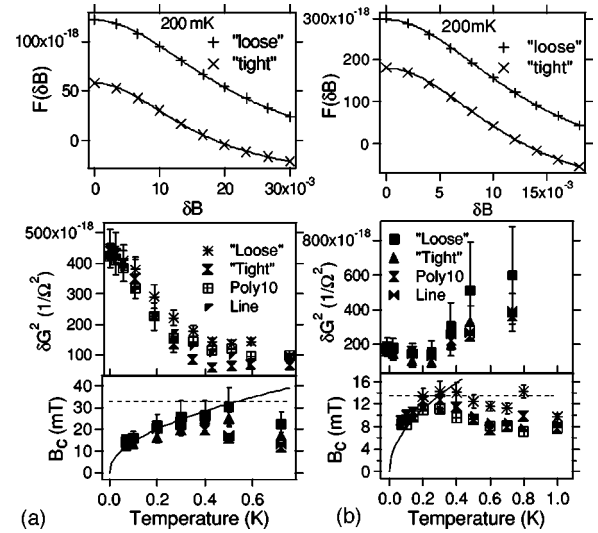


FIG. 4. (a) Results for  $\nu=1$ . (b) Results for  $\nu=2$ . Top: Correlation function for two different mean removal methods. The symbols are the data and the solid lines are fits to a Lorentzian plus a constant. The constants are different for the two mean removal methods, but the variance and  $B_c$  are similar. Middle: Variance vs  $T$ . Bottom:  $B_c$  vs  $T$ . The solid lines show a  $T^{1/2}$  dependence. The dashed lines show approximately where  $B_c$  flattens out as  $T$  increases to the point where  $B_c$  is set by  $A_1^*$ . In the legend, “loose” refers to the mean removal method of taking a running average over a long field range, “tight” refers to the running average method over a short field range, “poly10” is a 10th order polynomial mean removal method, and “line” refers to mean removal by subtracting a linear fit to  $G_{zz}(B)$  across the QH state.

In the  $\nu=2$  QH state, Fig. 4 shows that the variance,  $\langle \delta G^2 \rangle$ , decreases with increasing temperature for  $T < 500$  mK. At  $T > 500$  mK the variance levels off and changes little with increasing  $T$ . At low  $T$ , the corresponding  $B_c$  increases, as we expect, but for  $T > \sim 400$  mK, the correlation field saturates.

In the  $\nu=1$  QH state, the behavior of  $\langle \delta G^2 \rangle$  is different. At  $T < 300$  mK, the variance decreases weakly as  $T$  increases, but above 300 mK this trend reverses and the variance increases with  $T$ . As for  $\nu=2$ ,  $B_c$  initially increases steadily with  $T$ , but appears to stop growing for  $T$  above  $\sim 500$  mK.

We attempt to understand our results in terms of theories for transport on the chiral sheath.<sup>14,15</sup> Most studies of conductance fluctuations are done on isotropic, diffusive, metallic (degenerate) samples. In such systems, there is a single dephasing length  $l = (D\tau_\phi)^{1/2}$ , where  $D$  is the diffusion constant and  $\tau_\phi$  is the phase-breaking time. The dephasing time  $\tau_\phi$  produces two dephasing lengths in the anisotropic edge state sheath:<sup>14</sup>  $l_p = v_p\tau_\phi$  along the path of the edge states, where  $v_p$  is the electron’s edge velocity; and  $l_z$ , a vertical dephasing length. In the vertical ( $z$ ) direction, perpendicular to the layers, charge moves in a random walk. For  $l_z \gg a$ , the layer spacing,  $l_z = (D_z\tau_\phi)^{1/2}$ , where  $D_z$  is the diffusion constant in the vertical direction.

Theories of conductance fluctuations of the chiral sheath regard it as an array of phase-coherent “patches,” with dimensions  $l_p$  by  $l_z$ , that fluctuate independently. Treating the

patches as a network of random resistors yields expressions for variance and  $B_c$  that have different dependences<sup>14,15</sup> on  $l_z$  and  $l_p$  for different ratios of  $l_z$  to vertical length scales and of  $l_p$  to the distance,  $P$ , around the sheath (along the edge states). The earlier work<sup>14</sup> assumes uniform interedge tunneling around the sheath. This limit is unlikely to apply to our samples, due to the relative meander of adjacent edge states. In the presence of such meander, interedge tunneling will be nonuniform around the sheath, with large contributions from regions where adjacent edges cross over each other. For this reason, we focus on results of more recent theoretical work<sup>15</sup> that generalize to the case of strongly varying interedge tunneling.

Recent theory for transport on the chiral sheath<sup>15</sup> treats two limits: strongly coupled edges, for which  $l_p \gg l_\perp$ , and weakly coupled edges, for which  $l_p < l_\perp$ , where  $l_\perp \approx (aPe^2/h)/HG$  is the characteristic distance along the edge for interedge tunneling.<sup>16</sup> In the strongly coupled limit, the form of the correlation function is highly non-Lorentzian, while we observe that a Lorentzian fits our data well. Thus the weakly coupled limit appears to be more relevant to our data. This limit applies in the presence of relative edge meander if the flux linked by the vertical field between cross-over points of meandering adjacent edges is much less than a flux quantum.<sup>16</sup> Previous observations of different conductivities for in-plane fields oriented parallel and perpendicular to the mesa walls<sup>17</sup> indicate that the multilayers studied here are in the small-flux limit, as the large-flux limit would produce no anisotropy in the response of the multilayer to in-plane fields.

In the weakly coupled limit,  $l_p \ll l_\perp$ , a phase-coherent region has length  $l_p$  around the perimeter, and height  $a$ . Treating the sheath as an  $n_p = P/l_p$  by  $N_{\text{layer}}$  parallel-series network of random, classical resistors<sup>14,15</sup> yields variance

$$\langle \delta G_{zz}^2 \rangle = (\langle G_{zz} \rangle^2 / N_{\text{layer}}) (l_p / P), \quad (1)$$

where  $N_{\text{layer}} = 50$  is the number of periods in the multilayer and  $P$  is the distance around the sheath, along the edge states. The corresponding correlation function is Lorentzian.<sup>15</sup> If an in-plane field component perpendicular to the mesa walls drives the conductance fluctuations, the correlation field of the fluctuations is  $B_c = \phi_0 / (2\pi l_p a)$ , where the flux quantum  $\phi_0 = h/e$ .

Here the field,  $B$ , is applied perpendicular to the layer planes rather than perpendicular to the mesa walls. This ‘‘vertical’’ field orientation does not change the counting arguments that lead to Eq. (1). However, due to flux cancellation effects, it does affect the dependence of the correlation field,  $B_c$ , on  $l_p$ . The different in-plane meander of edge states in adjacent layers causes their projections onto the plane to cross, as sketched in Fig. 1(b). In the  $i$ th region between crossings of edge states,  $\phi_i = \pm BA_{i,\pm}$  is the flux linked through the in-plane area  $A_{i,\pm}$ . The  $\phi_i$  alternate in sign on each projected crossing of the edge states. The total flux through a phase-coherent region is  $\phi = BA_{\text{tot}}$ , where the net area that links flux is

$$A_{\text{tot}} = \sum_{i=1}^{N_+} A_{i,+} - \sum_{i=1}^{N_-} A_{i,-}. \quad (2)$$

The sums are over the  $N_+$  areas  $A_{i,+}$  and the  $N_-$  areas  $A_{i,-}$  within a phase-coherent region.

We assume that the individual terms  $A_{+,i}$  and  $A_{-,i}$  in Eq. (2) are each drawn from the same distribution  $P(A_1)$  of individual (positive) areas,  $A_1$ . As the number of terms in Eq. (2) increases, the distribution of total areas,  $P(A_{\text{tot}})$ , approaches a zero-mean Gaussian,  $P(A_{\text{tot}}) \propto \exp(-A_{\text{tot}}^2 / 2A_{\text{tot}}^{*2})$ . For simplicity we take the single-area distribution  $P(A_1) \propto \exp(-A_1 / 2A_1^*)^2$ , where  $A_1^*$  is the characteristic single area [other monotonically decaying forms, such as a simple exponential  $P \propto \exp(-A_1 / A_1^*)$ , yield similar results in the analysis below]. The width of the distribution  $P(A_{\text{tot}})$  of total areas is  $A_{\text{tot}}^* \sim N^{1/2} A_1^*$ , where  $N$  is the number of terms in either of the sums in Eq. (2).

Because the correlation function  $F(\Delta B) = F(-\Delta B)$ , positive and negative  $A_{\text{tot}}$  yield the same correlation field, which corresponds to the change in  $B$  that changes the flux linked through a phase-coherent area by roughly one flux quantum:  $B_c A_{\text{tot}} \sim h/e$ . For a phase coherence length  $l_p$  the number of terms in Eq. (2) is approximately  $N = l_p / L_{\text{cross}}$ , where  $L_{\text{cross}}$  is the average distance between crossings of adjacent edge states [Fig. 1(b)]. In the low- $T$  limit of large  $N$ ,  $A_{\text{tot}}^* \approx (l_p / L_{\text{cross}})^{1/2} A_1^*$  is the characteristic area for the distribution  $P(A_{\text{tot}})$ , so we expect  $B_c \approx (h/e) / A_{\text{tot}}^*$  to be the field scale characteristic of  $F(\Delta B)$ . Thus at low  $T$ ,  $B_c \approx (h/e) / [A_1^* (L_{\text{cross}} / l_p)^{1/2}]$ . If  $l_p \propto 1/T$ , as previously predicted using qualitative arguments for the chiral sheath,<sup>14</sup> then  $B_c \sim T^{1/2}$  at low temperatures. This result is consistent with the low-temperature behavior in Fig. 4, where the solid lines show a  $T^{1/2}$  dependence. At higher temperatures that give  $N \approx 1$ , flux cancellation will not be effective and  $B_c$  will be set by  $A_1^*$ , the area characteristic of the individual area distribution  $P(A_1)$ , so that  $B_c \approx (h/e) / A_1^*$ . The plots of  $B_c$  in the bottom row of Fig. 4 suggest that in this intermediate temperature regime,  $B_c \approx 30$  mT at  $\nu = 1$ , corresponding to  $A_1^* \approx 1.4 \times 10^{-13}$  m<sup>2</sup>; and  $B_c \approx 15$  mT at  $\nu = 2$ , corresponding to  $A_1^* \approx 2.7 \times 10^{-13}$  m<sup>2</sup> (two sets of edge states contribute to the fluctuations at  $\nu = 2$ , so a larger  $A_1^*$  seems reasonable). At still higher  $T$ ,  $\Delta B_c$  should grow as the phase-coherent area drops well below  $A_1^*$ . Based on the plots of  $B_c$  in Fig. 4, such a high- $T$  regime is not reached below 1 K.

We now turn to the  $T$ -dependent variances we observe at  $\nu = 1$  and  $\nu = 2$ .

The temperature dependence of the mean apparent in Fig. 2 complicates comparison of the data to the existing single-particle theories for the chiral sheath. These theories yield a  $T$ -independent mean, so the rise in  $\langle G_{zz} \rangle$  with  $T$  shown in Fig. 2 is not encompassed by currently available models for fluctuations of the chiral sheath. Thus, use of the  $T$ -dependent mean in Eq. (1) is of questionable validity; however, we do so for simplicity and in the absence of any more complete model.

Figure 5 plots the variance normalized by  $\langle G_{zz} \rangle^2$ . As shown,  $\langle \delta G_{zz}^2 \rangle / \langle G_{zz} \rangle^2$  falls monotonically with increasing  $T$ ,

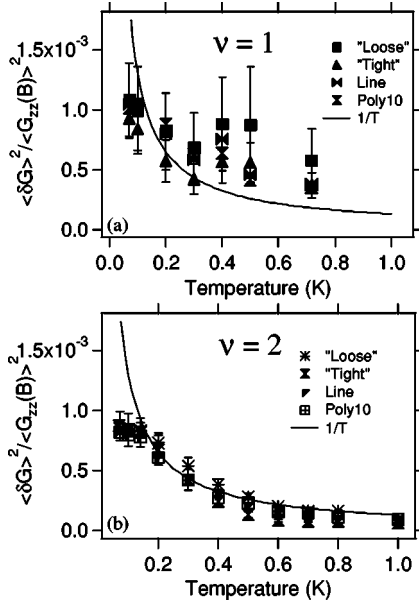


FIG. 5. (a) and (b)  $\langle \delta G_{zz}^2 \rangle / \langle G_{zz}(B) \rangle^2$  for  $\nu=1$  and 2. The solid lines show  $(C/T)$  with  $C=1.3 \times 10^{-4}$  K.

within error. Using Eq. (1) with  $P$  equal to  $P_0=20 \mu\text{m}$ , the nominal perimeter, gives  $l_p^{(0)} \approx 1 \mu\text{m}$  as the nominal dephasing length at 100 mK, in both QH states. This is much less than the  $l_\perp \sim 30 \mu\text{m}$  ( $15 \mu\text{m}$ ) at  $\nu=1$  ( $\nu=2$ ), also estimated using  $P=P_0$ . Thus the analysis yields  $l_p \ll l_\perp$ , as required for validity of Eq. (1).

Interpretation of the values of characteristic areas and lengths derived from the preceding analysis depends upon the structure at the edge. Impurities, defects, and sidewall roughness will likely make the actual paths of adjacent edge states resemble the banks of a meandering creek that necks down to small widths at the projected edge crossings [Fig. 1(b)]. In this case the distance  $P$  around the sheath, along the path of the edge states, can be substantially larger than the nominal mesa perimeter  $P_0$ , so that the phase coherence length along the edge states exceeds the  $l_p^{(0)}$  estimated above by a factor of roughly  $P/P_0$ . This same meander effect makes it possible for large areas  $A_1$  to accumulate between adjacent edge states over small distances along the nominal perimeter,  $P_0$ .

Studies of two-dimensional quantum Hall systems yield values of edge state phase coherence lengths ( $L_\phi$ ) of approximately  $100 \mu\text{m}$ , two orders of magnitude longer than the estimated  $l_p^{(0)} \sim 1 \mu\text{m}$  in our three-dimensional system.<sup>18</sup> These earlier studies of high-mobility two-dimensional electron gases (2DEGs) probed phase decoherence due to disorder-assisted electron-electron interactions that may be suppressed in these clean materials relative to disorder-assisted interactions in our much lower mobility samples (the samples studied in Ref. 19 had mobilities of roughly  $800\,000 \text{ cm}^2/\text{Vs}$ , or 30 times greater than the samples studied here). Our layered system also differs from 2DEGs in that charge fluctuations in one edge state couple to those in other edge states, providing an additional dephasing mechanism. For these reasons  $l_p$  in multilayers should be smaller

than  $L_\phi$  in high-mobility 2DEGs. We also expect that the path of the edge states will meander more in the multilayer mesas than the edge states in clean 2DEGs, so that the nominal  $l_p^{(0)}$  of the multilayer is reduced relative to  $L_\phi$  in 2DEGs by this geometrical effect.

Assuming that it is valid to normalize the variance by a  $T$ -dependent mean, the predicted<sup>14</sup>  $l_p \propto T^{-1}$  would yield  $\langle \delta G_{zz}^2 \rangle / \langle G_{zz}(T) \rangle^2 \sim 1/T$ . The lines in Fig. 5 show  $C/T$  curves with the constant  $C=1.3 \times 10^{-4}$  K adjusted to give the best overall agreement with  $\langle \delta G_{zz}^2(T) \rangle / \langle G_{zz}(T) \rangle^2$  for both  $\nu=1$  and  $\nu=2$ . As shown,  $\langle \delta G_{zz}^2 \rangle / \langle G_{zz} \rangle^2$  at  $\nu=2$  agrees with a  $T^{-1}$  temperature dependence except at the lowest temperatures. For  $\nu=1$ , the data are mostly consistent with a  $C/T$  dependence, with the same  $C$  as for  $\nu=2$ , except at the lowest  $T$ . For both  $\nu=2$  and  $\nu=1$ , the slower than  $T^{-1}$  growth of  $\langle \delta G_{zz}^2 \rangle / \langle G_{zz} \rangle^2$  at the lowest  $T$  could perhaps reflect the onset of saturation of the electron temperature.

Another possible factor in the behavior we observe is parallel conduction through the bulk. At sufficiently high temperatures the bulk (hopping) conductance will become significant in comparison with the sheath conductance, invalidating analysis in terms of sheath transport alone. We have used size-scaling calculations of the conductance to determine that bulk transport through the  $5\text{-}\mu\text{m} \times 5\text{-}\mu\text{m}$  mesa should not contribute appreciably to  $G_{zz}$  at temperatures below 1 K; however, these estimates used results from samples with lateral dimensions of  $\sim 100 \mu\text{m}$ , much larger than the bulk localization length within QH states. If the bulk localization length approached the dimension of the much smaller samples studied here, the distinction between edge and bulk would no longer be meaningful.

To determine the bulk localization length, we studied 1-mm  $\times$  1-mm samples of the same multilayer material in the  $\nu=2$  QH state.<sup>19</sup> Analysis of the data in terms of models for two-dimensional systems yielded an in-plane bulk localization length  $\xi \sim 0.40 \mu\text{m}$  in the center of the QH state. We found that  $G_{zz}$  within the  $\nu=1$  QH state of the  $5 \mu\text{m} \times 5 \mu\text{m}$  sample studied here exhibited a stronger temperature dependence than in  $\nu=2$  (Fig. 2), as might arise from parallel transport through the bulk. However, estimates based on a rather small number of data points in the center of the  $\nu=1$  QH state indicate that  $\xi$  is comparable in the  $\nu=1$  and  $\nu=2$  QH states. In both cases the estimated in-plane localization length at the centers of the QH states is roughly a factor of ten smaller than the lengths of the sides of the  $5\text{-}\mu\text{m} \times 5\text{-}\mu\text{m}$  mesa. Thus it still seems reasonable to think of distinct bulk and surface regions.

In summary, the studies presented here address the temperature dependence of phase coherence within a quantized Hall state. The results for the temperature dependences of the variance and the correlation field are strikingly different from those found in metallic systems and in single-layer quantum Hall systems in transition regions between QH states. Taking into account the temperature dependence of the mean conductance and the effects of flux cancellation on the correlation field yields reasonable overall agreement of  $\langle \delta G_{zz}^2 \rangle / \langle G_{zz} \rangle^2$  and  $B_c(T)$  with a dephasing time  $\tau_\phi \propto T^{-1}$ . The low-temperature variance suggests a short nominal dephasing length,  $l_p^{(0)} \sim 1 \mu\text{m}$ . This value is consistent with the

weak temperature dependence we observe in the mean conductance,  $G_{zz}$  (Fig. 2), in that we see no experimental signs for the onset of strong localization in vertical transport. In the weakly coupled multilayer studied here, we expect self-intersection of phase-coherent sheath trajectories to yield an insulating (exponential) decay in  $\langle G_{zz} \rangle$  that sets in at temperatures for which  $l_p(T) > P$ .<sup>14</sup> The  $l_p^{(0)}$  that we estimate

from the low- $T$  variance using the nominal perimeter,  $P_0$ , is well below the  $P_0 = 20 \mu\text{m}$  of the smallest sample, in agreement with the weak temperature dependence we observe in the mean conductance.

We thank John Chalker and Leon Balents for helpful conversations. This work was supported by NSF DMR9700767 and NSF DMR0071956.

- 
- <sup>1</sup>P.A. Lee, A.D. Stone, and H. Fukuyama, Phys. Rev. B **35**, 1039 (1987).  
<sup>2</sup>D.P. Druist, P.J. Turley, K.D. Maranowski, E.G. Gwinn, and A.C. Gossard, Phys. Rev. Lett. **80**, 365 (1998).  
<sup>3</sup>D.P. Druist, K. Yoo, P.J. Turley, and E.G. Gwinn, Superlattices Microstruct. **25**, 181 (1999).  
<sup>4</sup>F. Hohls, U. Zeitler, and R.J. Haug, Phys. Rev. B **66**, 073304 (2002).  
<sup>5</sup>D.H. Cobden and E. Kogan, Phys. Rev. B **54**, R17 316 (1996).  
<sup>6</sup>T. Machida, S. Ishizuka, S. Komiyama, K. Muraki, and Y. Hirayama, Phys. Rev. B **63**, 045318 (2001).  
<sup>7</sup>J.K. Jain and S.A. Kivelson, Phys. Rev. Lett. **60**, 1542 (1988).  
<sup>8</sup>J.A. Simmons, S.W. Hwang, D.C. Tsui, H.P. Wei, L.W. Engel, and M. Shayegan, Phys. Rev. B **44**, 12 933 (1991).  
<sup>9</sup>P.C. Main, A.K. Geim, H.A. Carmona, C.V. Brown, T.J. Foster, R. Taboryski, and P.E. Lindelof, Phys. Rev. B **50**, 4450 (1994).  
<sup>10</sup>H.A. Walling, D.P. Dougherty, D.P. Druist, E.G. Gwinn, K.D. Maranowski, and A.C. Gossard, Physica E (Amsterdam) **12**, 132 (2002).  
<sup>11</sup>H.A. Walling, D.P. Dougherty, D.P. Druist, E.G. Gwinn, K. Maranowski, and A.C. Gossard (unpublished).  
<sup>12</sup>D.P. Druist, Ph.D. dissertation, University of California, 2001.  
<sup>13</sup>H.A. Walling, Ph.D. dissertation, University of California, 2003.  
<sup>14</sup>S. Cho, L. Balents, and M.P.A. Fisher, Phys. Rev. B **56**, 15 814 (1997).  
<sup>15</sup>J.J. Betouras and J.T. Chalker, Phys. Rev. B **62**, 10 931 (2000).  
<sup>16</sup>J. Chalker (private communication).  
<sup>17</sup>D.P. Druist, E.G. Gwinn, K.D. Maranowski, and A.C. Gossard, Phys. Rev. B **68**, 075305 (2003).  
<sup>18</sup>T. Machida, H. Hirai, S. Komiyama, T. Osada, and Y. Shiraki, Solid State Commun. **103**, 441 (1997).  
<sup>19</sup>H.A. Walling, E.G. Gwinn, K.D. Maranowski, and A.C. Gossard Phys. Rev. B (to be published).